Eur Radiol (2013) 23:2030–2041
DOI 10.1007/s00330-013-2772-7

VASCULAR-INTERVENTIONAL

Characterisation of carotid plaques with ultrasound elastography: feasibility and correlation with high-resolution magnetic resonance imaging

Cyrille Naim · Guy Cloutier · Elizabeth Mercure · François Destrempes · Zhao Qin · Walid El-Abyad · Sylvain Lanthier · Marie-France Giroux · Gilles Soulez

Received: 17 August 2012 / Revised: 19 November 2012 / Accepted: 20 December 2012 / Published online: 17 February 2013

Abstract
Objectives To evaluate the ability of ultrasound non-invasive vascular elastography (NIVE) strain analysis to characterise carotid plaque composition and vulnerability as determined by high-resolution magnetic resonance imaging (MRI).

Methods Thirty-one subjects with 50 % or greater carotid stenosis underwent NIVE and high-resolution MRI of internal carotid arteries. Time-varying strain images (elastograms) of segmented plaques were generated from ultrasonic raw radio-frequency sequences. On MRI, corresponding plaques and

Electronic supplementary material The online version of this article (doi:10.1007/s00330-013-2772-7) contains supplementary material, which is available to authorised users.

C. Naim · W. El-Abyad · S. Lanthier · M.-F. Giroux · G. Soulez
Department of Radiology, University of Montreal Hospital Center (CHUM), Montréal, Québec, Canada

C. Naim
e-mail: cyrillenaim@yahoo.ca

W. El-Abyad
e-mail: walid.el.abyad.chum@ssss.gouv.qc.ca

S. Lanthier
e-mail: sylanthier@gmail.com

M.-F. Giroux
e-mail: m_fgiroux@videotron.ca

C. Naim · G. Cloutier · M.-F. Giroux · G. Soulez
Department of Radiology, Radio-Oncology and Nuclear Medicine, and Institute of Biomedical Engineering, University of Montreal, Montréal, Québec, Canada

G. Cloutier
e-mail: guy.cloutier@umontreal.ca

C. Naim · G. Cloutier · E. Mercure · F. Destrempes · Z. Qin · W. El-Abyad · S. Lanthier · G. Soulez
University of Montreal Hospital Research Center (CRCHUM), Montréal, Québec, Canada

E. Mercure
e-mail: elizabeth.mercure@gmail.com

F. Destrempes
e-mail: francois.destrempes@crchum.qc.ca

Z. Qin
e-mail: zhao.qin@crchum.qc.ca

C. Naim · G. Cloutier · E. Mercure · F. Destrempes · Z. Qin
Laboratory of Biorheology and Medical Ultrasonics, University of Montreal Hospital Research Center (CRCHUM), Montréal, Québec, Canada

S. Lanthier
Department of Medicine, University of Montreal Hospital Center (CHUM), Montréal, Québec, Canada

G. Soulez (✉)
Department of Radiology, Centre Hospitalier de l'Université de Montréal (CHUM),
Hôpital Notre-Dame—Pavillon Lachapelle (Room B1038-A),
1560 Sherbrooke East,
Montréal, Québec, Canada H2L 4M1
e-mail: gilles.soulez.chum@ssss.gouv.qc.ca

components were segmented and quantified. Associations between strain parameters, plaque composition and symptomatology were estimated with curve-fitting regressions and Mann–Whitney tests.

Results Mean stenosis and age were 72.7 % and 69.3 years, respectively. Of 31 plaques, 9 were symptomatic, 17 contained lipid and 7 were vulnerable on MRI. Strains were significantly lower in plaques containing a lipid core compared with those without lipid, with 77–100 % sensitivity and 57–79 % specificity ($P<0.032$). A statistically significant quadratic fit was found between strain and lipid content ($P<0.03$). Strains did not discriminate symptomatic patients or vulnerable plaques.

Conclusions Ultrasound NIVE is feasible in patients with significant carotid stenosis and can detect the presence of a lipid core with high sensitivity and moderate specificity. Studies of plaque progression with NIVE are required to identify vulnerable plaques.

Key points

- *Non-invasive vascular elastography (NIVE) provides additional information in vascular ultrasound*
- *Ultrasound NIVE is feasible in patients with significant carotid stenosis*
- *Ultrasound NIVE detects a lipid core with high sensitivity and moderate specificity*
- *Studies on plaque progression with NIVE are required to identify vulnerable plaques*

Keywords Carotid artery plaque · Atherosclerotic plaque · Elastography · Ultrasound · Magnetic resonance imaging (MRI)

Introduction

The severity of carotid stenosis is a strong predictor of recurrent atheroembolic strokes in symptomatic patients [1], but it is not a reliable predictor of stroke incidence in asymptomatic patients [2]. Hence, appropriate management of asymptomatic patients remains controversial, warranting further risk stratification.

According to the coronary artery literature, risk stratification should involve identification of the vulnerable atherosclerotic plaque at elevated risk of causing an ischaemic event [3]. Pathology of culprit coronary plaques has been shown to be similar to that of symptomatic carotid plaques [4]. Identification of vulnerable plaques in carotid arteries has been attempted with a variety of imaging techniques that characterise plaque composition, morphology, molecular processes, or biomechanical properties. Computed tomography (CT) and positron emission tomography (PET)-CT were proposed to evaluate plaque composition and inflammation, respectively [5, 6]. B-mode echo-texture [7] and plaque volume measurement by ultrasound [8] were also tested to evaluate plaque vulnerability and evolution with statin therapy. Ultimately, multicontrast high-resolution magnetic resonance imaging (MRI) was found to be the most accurate non-invasive imaging technique to identify and quantify plaque components compared with histology [9, 10]. In addition, MRI-detected intraplaque haemorrhage and fibrous cap disruption were associated with plaque vulnerability [11]. Despite its high sensitivity and specificity for plaque morphology [9, 10, 12, 13], elevated costs and time requirements render implementation of MRI difficult for patient screening and follow-up. As a result, an affordable non-invasive imaging technique to characterise carotid plaque composition and its progression is yet to be determined.

To date, there is no established technique analysing plaque biomechanics non-invasively. A previous ultrasound and MRI study demonstrated greater vessel wall compliance in common carotid arteries of healthy individuals compared with atherosclerotic arteries devoid of plaque [14]. Non-invasive vascular elastography (NIVE) by ultrasound is a novel technique that characterises plaque biomechanics by mapping carotid plaque strains (deformations) [15]. It is low-cost, implementable on modern clinical ultrasound machines and could potentially accompany routine carotid imaging examinations. A previous study assessed the feasibility of NIVE to analyse the strain of carotid walls in healthy subjects [16]. The next step is to evaluate the ability of NIVE strain analysis to characterise atherosclerotic plaques in patients with a carotid stenosis. We hypothesised that lipid-rich and vulnerable plaques have different strains than calcified and asymptomatic plaques. Hence, we aimed to evaluate the ability of ultrasound NIVE strain analysis to characterise carotid plaque composition and vulnerability, using high resolution MRI as a reference standard. As a secondary endpoint, we aimed to determine the feasibility of NIVE to discriminate vulnerable from asymptomatic patients.

Materials and methods

This prospective study was approved by the institutional review board. All subjects gave their written informed consent. Subjects were recruited from the vascular and interventional radiology, vascular surgery, neurology and vascular medicine clinics. From January 2006 to December 2010, 44 non-consecutive patients who had imaging of carotid arteries were enrolled. Carotid imaging was indicated in patients with new-onset ischaemic cerebrovascular symptoms, incidental findings of ischaemic disease on brain imaging, or for screening in the context of peripheral vascular disease. Men and women aged 40–85 years were eligible if they had a carotid artery stenosis of at least 50 % diameter reduction documented on colour and pulsed Doppler ultrasound or a

previous angiography study if available [CT angiography (n=23), MR angiography (n=4), digital subtraction angiography (n=1)]. Stenosis was evaluated according to the NASCET criteria [17] and ultrasound velocity profiles [18]. One carotid artery per patient was selected for analysis ("index side"): the symptomatic side, and for asymptomatic patients, the most severely stenotic side. Subjects were excluded if they had any contraindication to ultrasound, MRI or gadolinium injection; incomplete MRI or elastography examination; endarterectomy within the last 10 years; carotid stenting; total occlusion; or severe calcification that impeded proper ultrasound imaging.

At enrolment, a medical history and clinical examination were performed for all subjects. Baseline modified Rankin scale scores were recorded, and subjects were classified as vulnerable if they had a stroke or transient ischaemic attack (TIA) attributed to their index carotid artery plaque in the previous 3 months. If there was any doubt on the relationship between the occurrence of neurological symptoms and the index carotid, the patient was referred for an independent assessment by a neurologist. A colour and pulsed Doppler ultrasound examination was performed to confirm degree of stenosis, followed by an ultrasound acquisition for elastography on the same day and a high-resolution MRI of the index carotid artery within 1 month thereafter.

Asymptomatic subjects were followed clinically on annual basis in order to determine if their index carotid plaque became complicated (as would be expected of a vulnerable plaque), either in the form of a cerebrovascular event (stroke or TIA) in the territory of the index artery or a newly documented asymptomatic total artery occlusion. Subjects with complicated plaques were classified in the vulnerable group for analysis. No imaging to monitor plaque progression was performed unless prescribed by the treating physician.

Ultrasound elastography protocol

Ultrasound NIVE estimates the local deformation of a plaque induced by its natural cardiac pulsation, as explained schematically in Fig. 1.

A single operator performed all ultrasonic raw radiofrequency (RF) data sequence acquisitions, with an ES500RP system (Ultrasonix, Vancouver, Canada) equipped with a L14-5/38 linear array transducer. B-mode loop sequences from reconstructed RF data were acquired longitudinally at the level of the carotid bulb and plaque, over approximately 10 s. Blood pressure was recorded.

The implemented NIVE algorithm consisted firstly of a manual segmentation of the plaque on the first image frame, followed by automatic adaptation of the initialised region through the time-varying sequence [19]. The segmentation was performed by a technician and reviewed by a radiologist, both blinded to MRI. Second, the Lagrangian Speckle Model Estimator (LSME) algorithm [20] was applied to compute axial strain in the loop sequence of the segmented plaque. This algorithm calculates relative axial strain over time. Hence, for each image frame, an elastogram (colour map of axial strain) was obtained, and strain parameters were computed from the average axial strain of the whole plaque (Fig. 1). Time-varying strain curves were filtered to eliminate respiratory and motion artefacts ["Quantitative parameter extraction from axial strain maps in non-invasive vascular elastography of carotid arteries" by Mercure E, Destrempes F et al., presented at the 3rd MICCAI Workshop on Computing and Visualisation for (Intra) Vascular Imaging, 2011] and two to five consecutive cardiac cycles were chosen for analysis. A thorough biomechanical description of axial strain was obtained with four different strain parameters as outcome variables of NIVE: mean strain at peak systolic compression (MSPSC), mean strain amplitude (MSA), and maximal and minimal strain rates (MaxSR, MinSR). Figure 2 explains each parameter in detail.

MR imaging protocol

Using a 1.5-Tesla MRI unit (Siemens, Avanto, Erlangen, Germany) and a dedicated four-element RF surface coil, axial images of the index carotid artery were obtained from 10 mm below to 3 cm above the bifurcation. First, a three-dimensional (3D) time-of-flight sequence was performed. Using the same positioning, four black-blood double-inversion recovery turbo spin echo sequences were acquired in the following order: T2-weighted, proton density weighted, and pre- and post-contrast T1-weighted (Supplementary Table 1). Two adjacent slices containing the major portion of the plaque were selected for post-contrast imaging. Gadolinium-BOPTA (MultiHance, Bracco Diagnostics, Vaughan, ON, Canada) was injected at a rate of 2 ml/s (0.1 mmol/kg), after which image acquisition was performed every minute for 10 min. Slices were 3 mm-thick with 1 mm intersection gap. Total imaging time was typically less than 45 min.

MR image review

Plaque image analysis and segmentation were performed by one junior reader (6 months training) and reviewed by a senior reader (20 year experience in MR vascular imaging), after which a consensus reading was obtained. Both were blinded to plaque strain values and elastograms. All image sequences were used for interpretation and segmentation, including the post-contrast image sequence of the major plaque portion, which complemented plaque characterisation. The enhanced image sequence chosen for analysis was acquired at least 5 min after injection onset and displayed the best image quality and

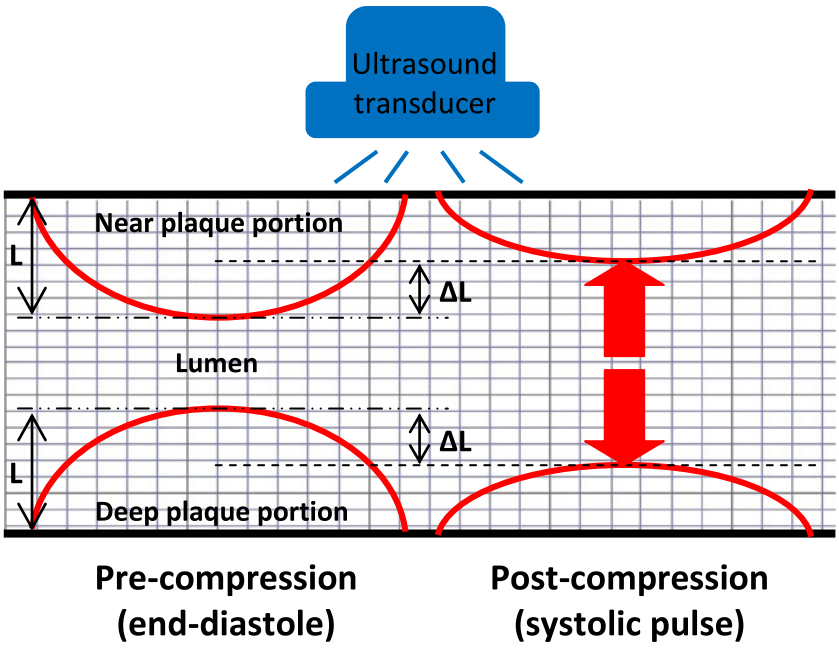

Fig. 1 Schematic depiction of ultrasound NIVE. Blood pressure from the systolic carotid pulse induces a compression (axial stress denoted by large *red arrows*) and a deformation (axial strain denoted by $\Delta L/L \times 100$) of the atherosclerotic plaque. This is a simplified depiction, because axial strain is calculated for each individual window (1.54×2.99 mm), after which mean axial strain for the entire segmented plaque is calculated

maximum enhancement. At each image slice level, vessel contours and components were manually traced using a segmentation software program (QPlaque MR 1.0.16, Medis, Netherlands) that provides volume and area measurements. Plaque components were identified using previously published criteria [9, 10, 12, 21], and included: lipid core, calcifications, intraplaque haemorrhage, loose matrix, fibrous cap and inflammation/neovasculature. Inflammation/neovasculature was defined as a region of enhancement on the post-contrast injection sequence [22]. Fibrous tissue was not segmented; it was defined as the remainder of the plaque between inner and outer vessel wall contours. Figure 3 illustrates a segmented plaque.

The carotid plaque was deemed vulnerable on MRI if it had one of the following features: thin fibrous cap with a large lipid core (≥25 % surface area), ruptured fibrous cap, or intraplaque haemorrhage (Fig. 3). The main outcome variables for high-resolution MRI were lipid and calcium proportions, in percentage of total plaque volume ("% lipid volume" and "% calcium volume").

Statistical analysis

Statistical tests were performed with IBM SPSS Statistics Standard software, version 19 (IBM, Armonk, NY). Comparisons between vulnerable and asymptomatic subjects were performed using Student *t*-tests (or Mann–Whitney when applicable), Pearson χ^2 and Fisher's exact tests.

Strain parameters were compared between plaques with and without calcium or lipid with Mann–Whitney tests. Receiver operating characteristic (ROC) curves were generated to determine sensitivity and specificity to detect plaques that contain lipid or calcium.

A multivariate analysis was performed to test association between strain and % lipid or calcium volume. Potential confounding variables tested included: age, gender, % stenosis, heart rate, and mean diastolic and systolic blood pressures. The level of significance was set at $P=0.05$.

Results

Forty-four subjects were recruited. Thirty-one met inclusion criteria for analysis as the flowchart demonstrates (Fig. 4). No adverse events occurred. Population baseline clinical, MRI and ultrasound characteristics are presented in Table 1. During a mean follow-up of 70 weeks (SD 82; range 27–254), one of the 23 asymptomatic subjects developed an asymptomatic total artery occlusion and was classified as vulnerable.

For three NIVE parameters, absolute strain values were significantly lower in atherosclerotic plaques containing a lipid core compared with those devoid of lipid (Table 2). Figure 5 shows the corresponding receiver operating characteristic (ROC) curves. To detect a lipid core, sensitivities and specificities ranged from 77 % to 100 % and 57 % to 79 %, respectively. For preventive medical therapy, sensitivity is sought. Thus, for MSPSC, MaxSR and MinSR, sensitivities of 88.2 %, 94.1 % and 100% with corresponding specificities of 57.1 % were obtained for strain value thresholds of 0.254 %, 1.834 % × s^{-1}, and −2.380 % × s^{-1}, respectively. On the other hand, for surgical therapy, specificity is preferred. Thus, specificities of 71.4 %, 78.6 %, and 78.6 %, with corresponding sensitivities of 76.5 %, 76.5 %, and 94.1 %, respectively, were obtained for strain value thresholds of 0.212 %, 1.440 % × s^{-1}, and −2.099 % × s^{-1}.

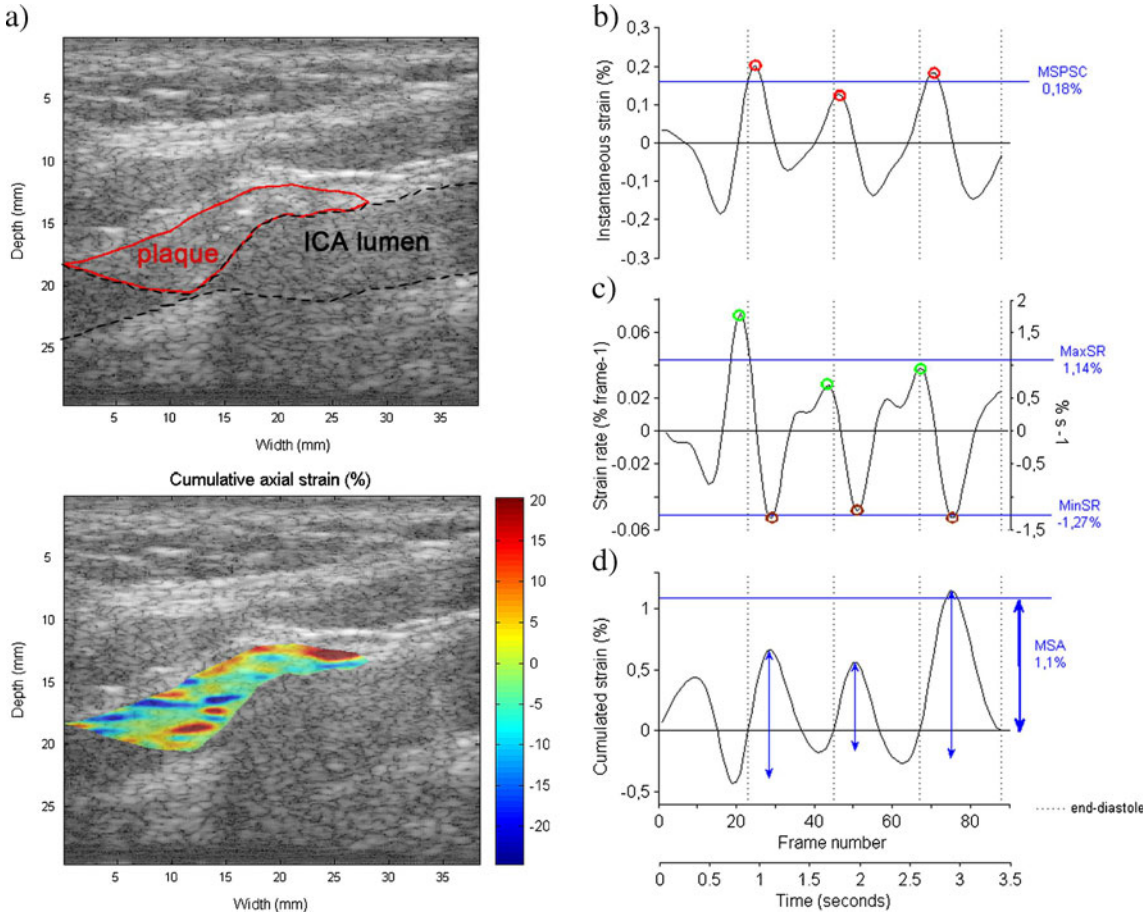

Fig. 2 Elastogram and strain curves of the left carotid plaque of a 70-year-old man who presented with left-sided amaurosis fugax. **a** A two-dimensional longitudinal view B-mode image reconstructed from raw RF data showing the segmented plaque (*red contour*) on the anterior vascular wall of the internal carotid artery (*ICA*), and the same image with a superimposed elastogram (colour map) representing cumulated axial strain at maximal systolic compression. The colours range from −20 % (*dark blue*) to +20 % (*dark red*), denoting areas of dilation and compression respectively. **b** A graph of instantaneous mean axial strain is obtained from the strain difference between two consecutive image frames, thus representing the variation of mean axial strain over time. Peak systolic compression is denoted by *red circles*. Mean strain at peak systolic compression (*MSPSC*) is the average of these peak values over the number of cardiac cycles. *Dotted vertical lines* represent end-diastole, estimated from B-mode videos and M-mode images. **c** Strain rate is the slope of the instantaneous strain in (**b**). Maximum strain rate (*MaxSR*) is the mean of the greatest strain rate occurring at end-diastole (*green circles*). Minimum strain rate (*MinSR*) is the mean of the lowest strain rate, occurring at the onset of diastole (*purple circles*). In other words, MaxSR represents greatest tissue compression over time, and MinSR represents greatest tissue dilation over time, which explains why MinSR is a negative value. **d** A graph of cumulated mean axial strains is derived from (**b**). *Double-sided blue arrows* represent strain amplitude for each cardiac cycle. Mean strain amplitude (*MSA*) is the average of these three amplitudes. The peak of the third cardiac cycle corresponds to the elastogram in (**a**)

NIVE strain parameters had no significant difference between vulnerable and non-vulnerable patients, genders, or presence and absence of calcium, inflammation, haemorrhage or ulceration. Also, strain parameters had no association with modified Rankin scale score, degree of stenosis, age, heart rate, and blood pressure, except for MSA correlating negatively with heart rate (Spearman correlation coefficient (r_s)=−0.385, P=0.036).

Curve-fitting analyses revealed significant quadratic correlations between the % lipid volume and each of the four NIVE parameters. On scatter plots, higher strains were observed with little to no lipid content, followed by an initial decrease in strain values until approximately 12 % lipid volume, after which strain values increased slightly with lipid content (Fig. 6). Only age and heart rate were found to have a confounding effect on these associations. Nevertheless, these associations maintained significance levels in multivariate analyses (Supplementary Table 2). An inverse correlation between % calcium volume and % lipid volume was found (r_s=−0.624, P=0.00009), but % calcium volume did not significantly change the nature or strength of the association between % lipid volume and each strain parameter.

There were borderline positive linear associations between % calcium volume and two strain parameters, MSA and MinSR; however these associations lost significance when controlling for confounding variables (Supplementary Fig. 1

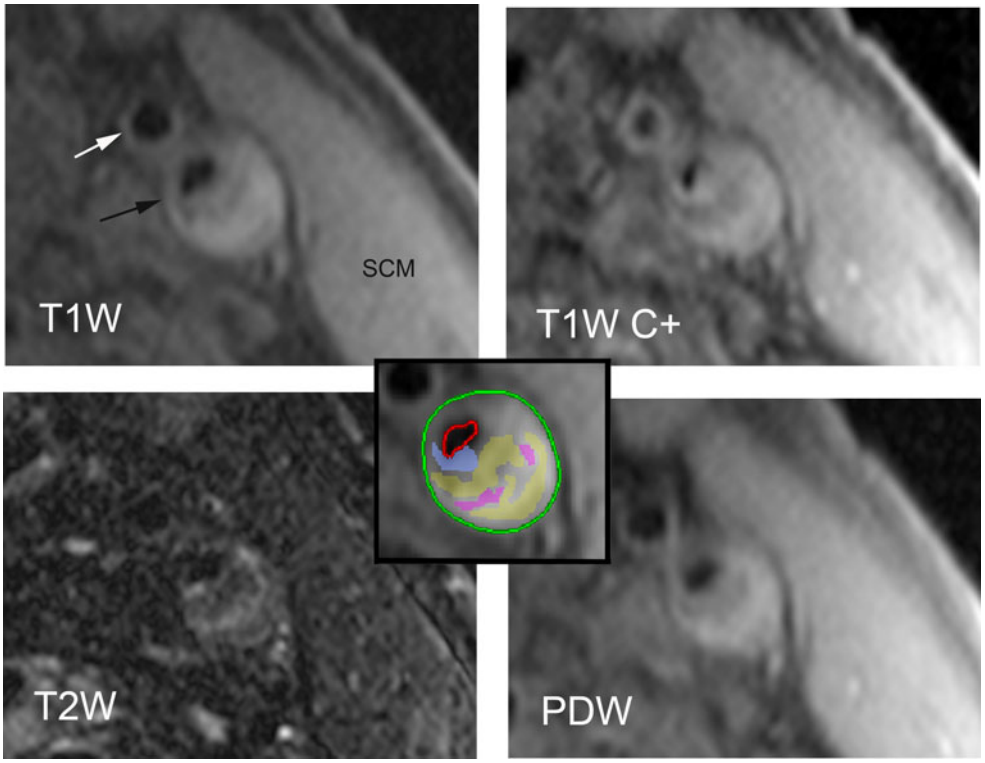

Fig. 3 High-resolution MRI of the left internal carotid artery plaque of a 65-year-old man who presented with a left hemispheric stroke (axial view). This is a vulnerable-appearing lipid-rich haemorrhagic plaque. The external and internal carotid arteries are indicated with a *white and black arrow*, respectively. The segmentation using the QPlaque software is shown superimposed on the T1-weighted image (framed inset at the centre). The *green and red contours* designate the outer and inner vascular wall contours of the internal carotid artery. *Yellow* represents lipid, *pink* represents haemorrhage and *purple* represents inflammation. *T1W* T1-weighted, *T2W* T2-weighted, *PDW* proton density-weighted, *T1WC+* T1-weighted post-contrast injection

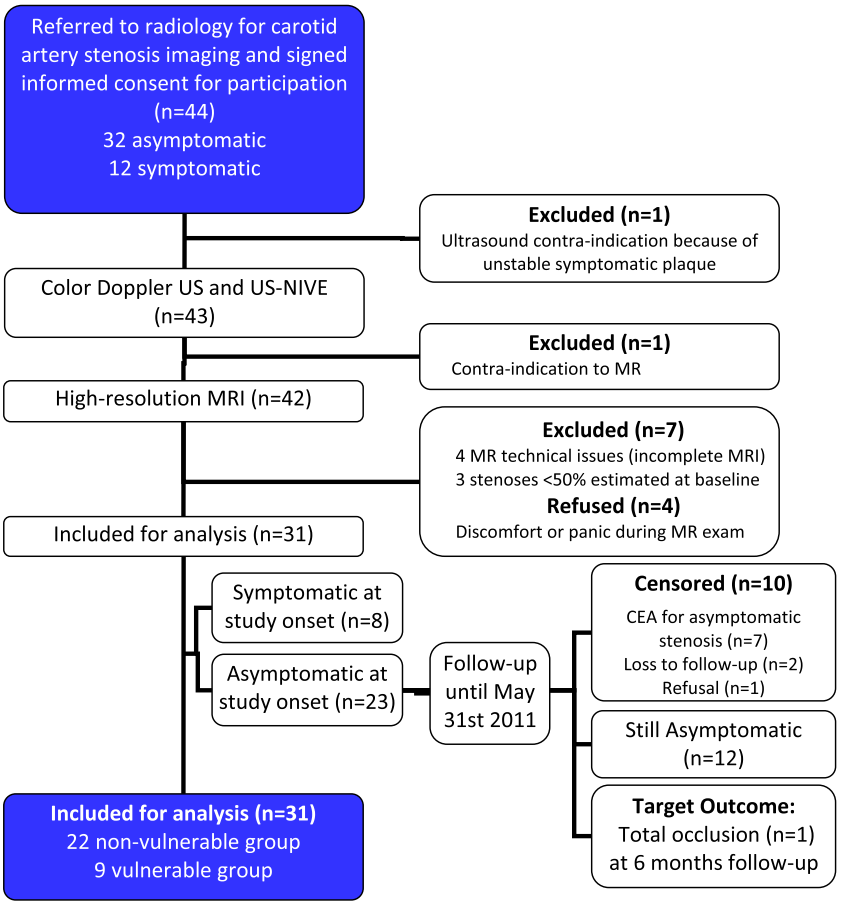

Fig. 4 Flowchart of subject recruitment

Table 1 Population characteristics

		Total n=31	Vulnerable n=9	Non-vulnerable n=22	P value
Clinical characteristics					
Male (number) [a]		22 (71 %)	8 (88.9 %)	14 (63.6 %)	0.160
Age (years) [d]		69.3±7.8	69.3±9.0	69.3±7.5	0.793
Mean percent diameter stenosis (%) [d]		72.7±12.2	74.4±12.4	72.1±12.4	0.544
Vulnerable		9 (29 %)			
Amaurosis fugax		3			
TIA		1			
Completed stroke		3			
Retinal infarct		1			
Asymptomatic carotid occlusion		1			
Body mass index (kg/m^2) [c]		26.6±4.5	28.2±6.0	26.0±3.8	0.246
Peripheral vascular disease [a]		22 (71 %)	2 (22.2 %)	20 (90.9 %)	0.0001[f]
Ischaemic heart disease [a]		12 (38.7 %)	3 (33.3 %)	9 (40.9 %)	0.694
Diabetes mellitus [a]		15 (48.4 %)	5 (55.6 %)	10 (45.5 %)	0.609
Dyslipidemia [a]		27 (87.1 %)	7 (77.8 %)	20 (90.9 %)	0.322
Hypertension [a]		27 (87.1 %)	6 (66.7 %)	21 (95.5 %)	0.030[f]
Smoking history [a]		25 (80.7 %)	7 (77.8 %)	18 (81.8 %)	0.965
Rankin scale [e a]	0	23 (74.2 %)	5 (55.6 %)	18 (81.8 %)	0.039[f]
	1	4 (12.9 %)	3 (33.3 %)	1 (4.5 %)	
	2	3 (9.7 %)	0 (0.0 %)	3 (13.6 %)	
	3	1 (3.2 %)	1 (11.1 %)	0 (0.0 %)	
Serum biochemistry [d]		3.85±0.82	3.87±1.11	3.84±0.71	0.826
Total cholesterol (C) (mmol/l)					
LDL-C (mmol/l)		2.00±0.70	2.11±1.04	1.97±0.54	0.807
C-reactive protein (mg/l)		4.01±3.20	3.02±1.72	4.30±3.51	0.670
Mean sBP (mm Hg) [c]		132.3±16.3	120.2±12.2	137.1±15.4	0.007[f]
Mean dBP (mm Hg) [c]		67.3±10.0	66.9±10.3	69.3±10.1	0.553
Mean pulse (beats per minute) [c]		69.7±14.8	73.6±18.1	69.8±13.5	0.530
MRI characteristics					
Lipid [b]		17 (54.8 %)	7 (77.8 %)	10 (45.5 %)	0.132
Calcium [b]		27 (87.1 %)	8 (88.9 %)	19 (86.4 %)	1.000
Intra-plaque haemorrhage[b]		2 (6.5 %)	2 (22.2 %)	0 (0 %)	0.077
Contrast enhancement [a]		19 (61.3 %)	6 (66.7 %)	13 (59.1 %)	0.694
Fibrous cap [a]					
Thick intact		24 (77.4 %)	5 (55.6 %)	19 (86.4 %)	0.019[f]
Thin Intact		2 (6.5 %)	0 (0 %)	2 (9.1 %)	
Ruptured		5 (16.1 %)	4 (44.4 %)	1 (4.5 %)	
Vulnerable-appearing [a]		7 (22.6 %)	4 (44.4 %)	3 (13.6 %)	0.063
Modified AHA criteria [a] [22]					
Type IV-V, fibroatheroma		10 (32.3 %)	3 (33.3 %)	7 (31.8 %)	0.019[f]
Type VI, complicated		5 (16.1 %)	4 (44.4 %)	1 (4.5 %)	
Type VII, calcified		9 (29.0 %)	0 (0.0 %)	9 (40.9 %)	
Type VIII, fibrous		7 (22.6 %)	2 (22.2 %)	5 (22.7 %)	
Mean % volumes					
Lipid [d]		4.8±9.3	9.4±11.3	3.0±7.9	0.022[f]
Calcium [c]		5.1±4.6	2.2±2.5	6.3±4.8	0.005[f]
Intra-plaque haemorrhage[d]		0.05±0.2	0.2±0.3	0.0±0.0	0.025[f]

Table 1 (continued)

	Total n=31	Vulnerable n=9	Non-vulnerable n=22	P value
Ultrasound characteristics				
Degree of calcification [a]				
0=absent	7 (22.6 %)	4 (44.4 %)	3 (13.6 %)	0.176
1=slight	5 (16.1 %)	2 (22.2 %)	3 (13.6 %)	
2=moderate	9 (29.0 %)	2 (22.2 %)	7 (31.8 %)	
3=severe	10 (32.3 %)	1 (11.1 %)	9 (40.9 %)	
Plaque echogenicity [a]				
1=hypoechoic	8 (25.8 %)	3 (33.3 %)	5 (22.7 %)	0.0004[f]
2=isoechoic	2 (6.5 %)	2 (22.2 %)	0 (0.0 %)	
3=hyperechoic	16 (51.6 %)	0 (0.0 %)	16 (72.7 %)	
4=heterogeneous	5 (16.1 %)	4 (44.4 %)	1 (4.5 %)	

sBP systolic blood pressure, *dBP* diastolic blood pressure

[a] Pearson chi-squared test

[b] Fisher's exact test (bilateral)

[c] Independent sample Student *t*-test

[d] Mann–Whitney test

[e] Rankin scale at participation onset

[f] Statistically significant

and Supplementary Table 2). Finally, there were no significant correlations between percentage volumes of other plaque components and strain parameters.

Discussion

This study demonstrated the clinical feasibility of NIVE to characterise carotid plaque composition by strain analysis in patients with 50 % or greater stenosis. The NIVE algorithm used in our study is based on the Lagrangian Speckle Model Estimator that estimates the deformation of plaque components induced by the cardiac pulsation [20]. It does not require external compression or creation of a radiation force. Acoustic radiation force impulse imaging has previously been tested in phantoms, ex-vivo and in-vivo in carotid arteries but without clinical validation [23].

In this patient population, NIVE strain parameters (MSPSC, Max and MinSR) detected the presence of a lipid core with high sensitivity and moderate specificity. The ability to non-invasively detect a lipid core with NIVE in patients with significant stenoses can be valuable to identify vulnerable plaque and monitor pharmacotherapeutic effects on plaque stabilisation. Such a tool could also be helpful in determining which asymptomatic patients would benefit from surgical treatment.

We observed significantly lower strain values in carotid plaques that contained a lipid core. This contradicts findings from previous authors who observed higher strain values in

Table 2 Bivariate associations between strain and presence of lipid

Strain parameters	Strain values, Mean±SD			P value
	Median			
	Total n=31	Lipid present n=17	Lipid absent n=14	
MSPSC (%)	0.205±0.120 0.193	0.163±0.076 0.140	0.257±0.144 0.259	0.032[a]
MSA (%)	1.248±0.775 1.060	1.101±0.677 0.806	1.428±0.871 1.396	0.131
MaxSR (%s^{-1})	1.587±1.004 1.407	1.110±0.446 0.997	2.166±1.193 2.020	0.003[a]
MinSR (%s^{-1})	−1.841±1.199 −1.650	−1.234±0.585 −1.139	−2.578±1.354 −2.408	0.001[a]

MSA mean strain amplitude, *MSPSC* mean strain at peak systolic compression, *MaxSR* maximal strain rate, *MinSR* minimal strain rate

[a]Statistically significant

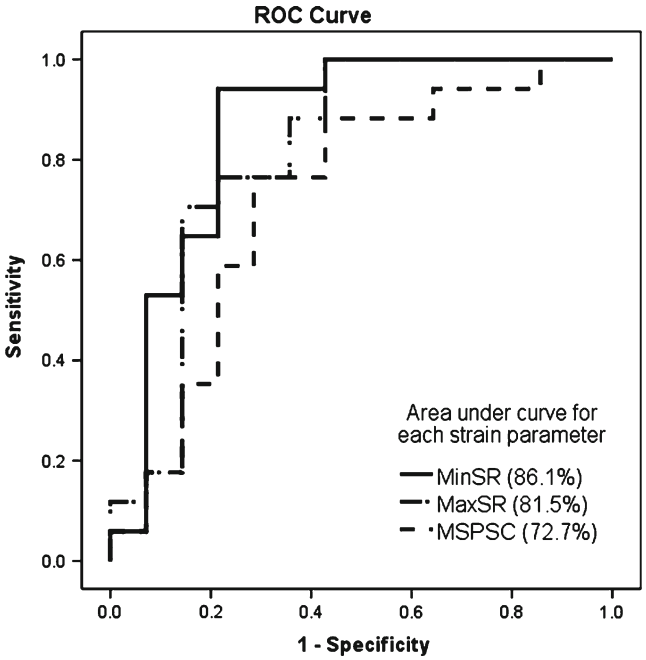

Fig. 5 ROC curves for NIVE strain parameters to detect the presence of a lipid core

early fatty plaques compared with non-fatty plaques using intravascular ultrasound elastography (IVUS) in iliac and femoral arteries of pigs [24]. In this last study, the types of atherosclerotic plaques were different from those of the present patient population: all fatty plaques were less than 30 % stenotic, homogeneous and devoid of calcium. Conversely, the present study included mostly heterogeneous large stenotic plaques with some degree of calcification. Given that strain parameters were spatially averaged on the whole segmented plaque, we interpret our findings with a "damper" hypothesis, whereby a lipid core embedded in a large plaque behaves as a damper reducing deformation of the whole plaque.

We observed non-linear U-shaped associations between axial strain indices and plaque lipid content. This quadratic fit is explained by the above finding where plaques containing lipid had smaller strains than those devoid of lipid. As the lipid core further increased in size above approximately 12 % lipid volume, there was a slight and steady increase in strain, but with values that remained lower than strains of plaques devoid of lipid (Fig. 6). The latter part of the association relies on a very small number of subjects, but concurs with previously published observations [24].

We observed a borderline significant tendency for MSA to increase and MinSR to decrease with calcium content. In contrast, previous authors reported lower strain values in calcified areas on in vivo ultrasound elastograms [25]. We previously found that the effect of a rigid calcium annulus could cause a high mechanical stress on other plaque components and induce high strain values around it [15]. Since we are averaging strain parameters within the whole plaque, this "hammer effect" may explain the large variability and slight rise in strain associated with calcium content. Detection of areas with elevated strain or high strain spatial variation may be valuable to identify areas of elevated shear stress and potential plaque rupture.

Strain parameters did not identify vulnerable subjects or vulnerable plaques by MRI criteria. This can partially be explained by the spatial averaging of strain parameters as discussed above. In addition, we did not study more sensitive surrogate endpoints of vulnerability such as subclinical ischaemic lesions on follow-up brain MRI or advanced neuropsychological testing [26], thus limiting the evaluation of vulnerability to hard clinical endpoints, which usually require a larger sample size to find meaningful differences. Finally, in contrast to the study by Maurice et al. [16] on normal subjects demonstrating higher strain values in women, we did not find gender differences. This may be attributed to our sample population, with a male predominance and advanced atherosclerotic disease.

Baseline clinical characteristics were similar among vulnerable and non-vulnerable subjects, except for a higher prevalence of peripheral vascular disease and hypertension in asymptomatic subjects. This can be explained by the recruitment of asymptomatic patients mainly from vascular surgery and interventional radiology clinics, and the strong association between peripheral vascular disease and hypertension [27].

Other imaging findings in symptomatic patients are consistent with previous studies, such as for MRI, a higher prevalence of plaque vulnerability features [28], higher lipid and lower calcium content [11, 29], and for ultrasound, lower plaque echogenicity [30].

Our study adds to earlier vascular elastography techniques by providing non-invasively four distinct strain parameters that showed consistent associations with lipid content. The strain parameters MSPSC and MSA used in this study were similar to those used in other studies, both in computation methodology and strain magnitude [15, 16, 24, 25, 31]. Finally, our study is the first to provide non-invasive strain analysis in vivo in patients with atherosclerotic carotid stenosis, with high-resolution multicontrast MRI as a reference standard for plaque composition.

The present ultrasound NIVE technique has limitations in the characterisation of atherosclerotic plaques. First, as described above, given that most atherosclerotic plaques are heterogeneous structures made of lipid and calcium, areas with high and low deformations are pooled together to compute mean strain. This evens out strain parameter values and consequently decreases the ability of NIVE to discriminate plaques based on mechanical behaviour. Second, most of the plaque consists of fibrous tissue. With a two-dimensional longitudinal acquisition, a limited B-mode image quality obtained from reconstructed RF signals, and no real time visualisation of elastograms, we could not target

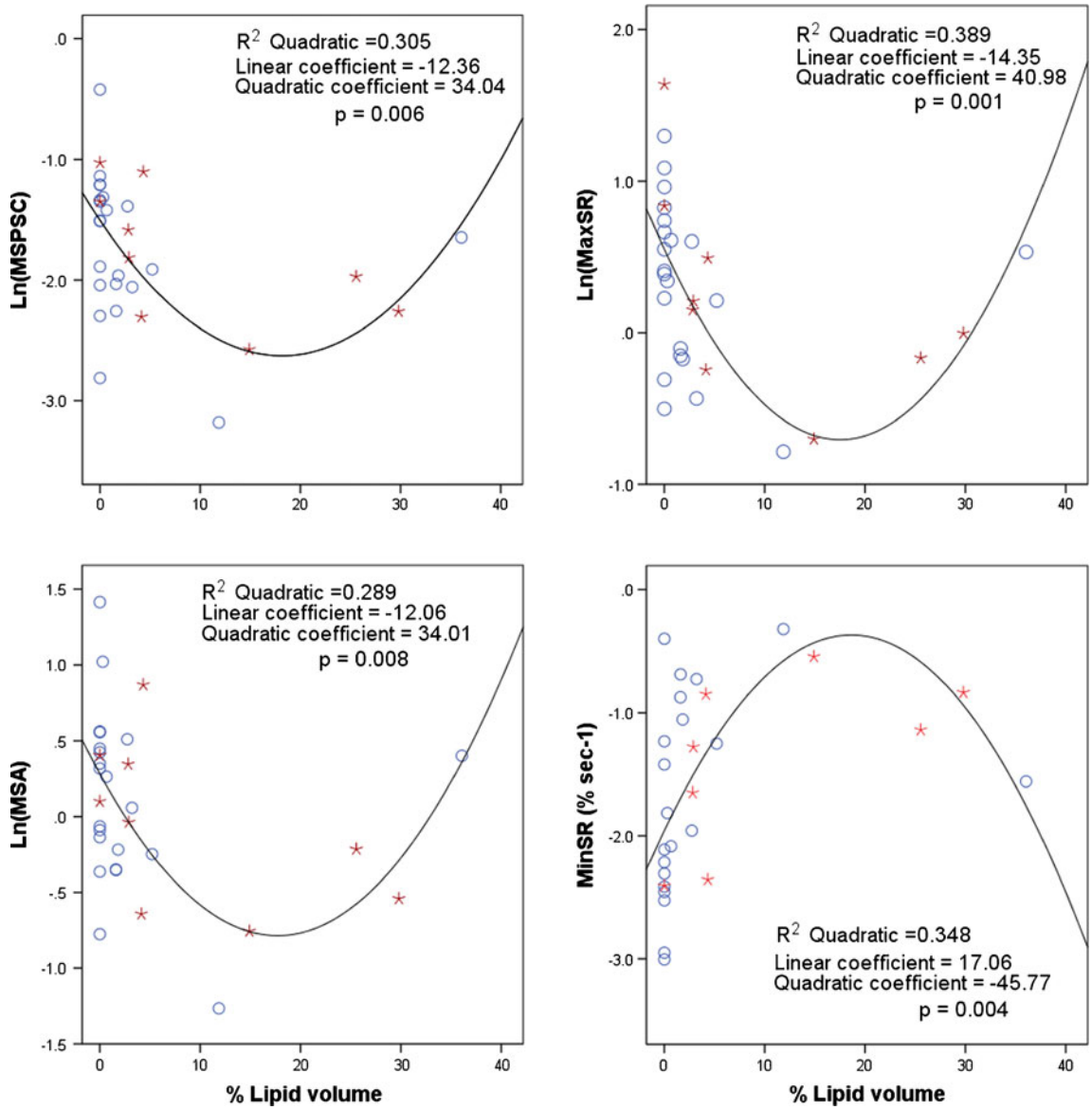

Fig. 6 Scatter plots with curve fitting functions of the natural logarithm of strain parameters with % lipid volume (bivariate analysis). Note that only for the MinSR parameter, two outliers were removed to normalise the distribution. For all other parameters, a natural logarithm was applied for normalisation. *MSPSC* mean strain at peak systolic compression, *MSA* mean strain amplitude, *MaxSR* and *MinSR* maximal and minimal strain rates; *red stars* symptomatic group, *blue circles* asymptomatic group

specific regions of interest within the plaque during image acquisition and segmentation. Further technical optimisation and analysis may provide NIVE with the ability to detect vulnerable plaque. The assessment of Young's modulograms with a priori information relying on elastography strain maps is an avenue deserving attention for such an objective [32].

This study provides a comprehensive evaluation of the current ultrasound NIVE technique and a better understanding of carotid plaque biomechanical behaviour associated with its content. In addition, it demonstrates the need for technical optimisation of strain analysis in order to ultimately detect vulnerability. Further studies with exploration of real-time imaging to visualise and target plaque components, echo-texture analysis based on raw RF signals, modulography and shear strain mapping could be valuable to improve plaque characterisation and detect vulnerability.

In conclusion, ultrasound NIVE is feasible and can detect the presence of a lipid core in subjects with significant carotid stenosis with high sensitivity and moderate specificity. Larger patient populations and further technical optimisation of ultrasound NIVE with real time imaging and plaque subcomponent analysis are required to better characterise the biomechanical behaviour of carotid atherosclerotic plaques.

Acknowledgments The authors are grateful to Mrs Vicky Thiffault, Louise Allard and Andrée Cliche for their dedication in study coordination, IRB documentation preparation and patient recruitment. We would like to also acknowledge the contributions of Drs Stéphane Elkouri, Nathalie Beaudoin, Jean-Francois Blair and Eric Therasse in patient recruitment and useful advices. We would also like to thank Madame Marie-Pierre Sylvestre, biostatistician, who guided us through statistical analyses. The authors are also grateful to the Natural Sciences and Engineering Research Council of Canada, the Canadian Institutes of Health Research, Gestion Univalor and Bracco Diagnostics who provided grants to help fund this project.

Dr Gilles Soulez holds a national scientist award from the Fonds de la Recherche en Santé du Québec.

References

1. Rothwell PM, Eliasziw M, Gutnikov SA et al (2003) Analysis of pooled data from the randomised controlled trials of endarterectomy for symptomatic carotid stenosis. Lancet 361:107–116
2. Halliday A, Harrison M, Hayter E et al (2010) 10-year stroke prevention after successful carotid endarterectomy for asymptomatic stenosis (ACST-1): a multicentre randomised trial. Lancet 376:1074–1084
3. Naghavi M, Libby P, Falk E et al (2003) From vulnerable plaque to vulnerable patient: a call for new definitions and risk assessment strategies: part I. Circulation 108:1664–1672
4. Redgrave JNE, Lovett JK, Gallagher PJ, Rothwell PM (2006) Histological assessment of 526 symptomatic carotid plaques in relation to the nature and timing of ischemic symptoms: the oxford plaque study. Circulation 113:2320–2328
5. de Weert TT, Ouhlous M, Meijering E et al (2006) In vivo characterization and quantification of atherosclerotic carotid plaque components with multidetector computed tomography and histopathological correlation. Arterioscler Thromb Vasc Biol 26:2366–2372
6. Tawakol A, Migrino RQ, Bashian GG et al (2006) In vivo 18F-fluorodeoxyglucose positron emission tomography imaging provides a noninvasive measure of carotid plaque inflammation in patients. J Am Coll Cardiol 48:1818–1824
7. Christodoulou CI, Pattichis CS, Pantziaris M, Nicolaides A (2003) Texture-based classification of atherosclerotic carotid plaques. IEEE Trans Med Imaging 22:902–912
8. Ainsworth CD, Blake CC, Tamayo A, Beletsky V, Fenster A, Spence JD (2005) 3D ultrasound measurement of change in carotid plaque volume: a tool for rapid evaluation of new therapies. Stroke 36:1904–1909
9. Cai J, Hatsukami TS, Ferguson MS et al (2005) In vivo quantitative measurement of intact fibrous cap and lipid-rich necrotic core size in atherosclerotic carotid plaque: comparison of high-resolution, contrast-enhanced magnetic resonance imaging and histology. Circulation 112:3437–3444
10. Cappendijk VC, Cleutjens KBJM, Kessels AGH et al (2005) Assessment of human atherosclerotic carotid plaque components with multisequence MR imaging: initial experience. Radiology 234:487–492
11. Takaya N, Yuan C, Chu B et al (2006) Association between carotid plaque characteristics and subsequent ischemic cerebrovascular events: a prospective assessment with MRI—initial results. Stroke 37:818–823
12. Yuan C, Mitsumori LM, Ferguson MS et al (2001) In vivo accuracy of multispectral magnetic resonance imaging for identifying lipid-rich necrotic cores and intraplaque haemorrhage in advanced human carotid plaques. Circulation 104:2051–2056
13. Fabiano S, Mancino S, Stefanini M et al (2008) High-resolution multicontrast-weighted MR imaging from human carotid endarterectomy specimens to assess carotid plaque components. Eur Radiol 18:2912–2921
14. Harloff A, Zech T, Frydrychowicz A et al (2009) Carotid intima-media thickness and distensibility measured by MRI at 3 T versus high-resolution ultrasound. Eur Radiol 19:1470–1479
15. Schmitt C, Soulez G, Maurice RL, Giroux MF, Cloutier G (2007) Noninvasive vascular elastography: toward a complementary characterization tool of atherosclerosis in carotid arteries. Ultrasound Med Biol 33:1841–1858
16. Maurice RL, Soulez G, Giroux MF, Cloutier G (2008) Noninvasive vascular elastography for carotid artery characterization on subjects without previous history of atherosclerosis. Med Phys 35:3436–3443
17. North American Symptomatic Carotid Endarterectomy Trial Collaborators (1991) Beneficial effect of carotid endarterectomy in symptomatic patients with high-grade carotid stenosis. N Engl J Med 325:445–453
18. Grant EG, Benson CB, Moneta GL et al (2003) Carotid artery stenosis: gray-scale and Doppler US diagnosis—Society of Radiologists in Ultrasound Consensus Conference. Radiology 229:340–346
19. Destrempes F, Meunier J, Giroux MF, Soulez G, Cloutier G (2011) Segmentation of plaques in sequences of ultrasonic B-mode images of carotid arteries based on motion estimation and a bayesian model. IEEE Trans Biomed Eng 58:2202–2211
20. Maurice RL, Ohayon J, Fretigny Y, Bertrand M, Soulez G, Cloutier G (2004) Noninvasive vascular elastography: theoretical framework. IEEE Trans Med Imaging 23:164–180
21. Cai J-M, Hatsukami TS, Ferguson MS, Small R, Polissar NL, Yuan C (2002) Classification of human carotid atherosclerotic lesions with in vivo multicontrast magnetic resonance imaging. Circulation 106:1368–1373
22. Kerwin WS, O'Brien KD, Ferguson MS, Polissar N, Hatsukami TS, Yuan C (2006) Inflammation in carotid atherosclerotic plaque: a dynamic contrast-enhanced MR imaging study. Radiology 241:459–468
23. Allen JD, Ham KL, Dumont DM, Sileshi B, Trahey GE, Dahl JJ (2011) The development and potential of acoustic radiation force impulse (ARFI) imaging for carotid artery plaque characterization. Vasc Med 16:302–311
24. de Korte CL, Sierevogel MJ, Mastik F et al (2002) Identification of atherosclerotic plaque components with intravascular ultrasound elastography in vivo. Circulation 105:1627–1630
25. Shi H, Mitchell CC, McCormick M, Kliewer MA, Dempsey RJ, Varghese T (2008) Preliminary in vivo atherosclerotic carotid plaque characterization using the accumulated axial strain and relative lateral shift strain indices. Phys Med Biol 53:6377–6394
26. Dempsey RJ, Vemuganti R, Varghese T, Hermann BP (2010) A review of carotid atherosclerosis and vascular cognitive decline: a new understanding of the keys to symptomology. Neurosurgery 67:484–494
27. Selvin E, Erlinger TP (2004) Prevalence of and risk factors for peripheral arterial disease in the United States: results from the National Health and Nutrition Examination Survey, 1999–2000. Circulation 110:738–743
28. Saam T, Cai J, Ma L et al (2006) Comparison of symptomatic and asymptomatic atherosclerotic carotid plaque features with in vivo MR imaging. Radiology 240:464–472
29. Nandalur KR, Baskurt E, Hagspiel KD, Phillips CD, Kramer CM (2005) Calcified carotid atherosclerotic plaque is associated less with ischemic symptoms than is noncalcified plaque on MDCT. AJR Am J Roentgenol 184:295–298

30. Mathiesen EB, Bonaa KH, Joakimsen O (2001) Echolucent plaques are associated with high risk of ischemic cerebrovascular events in carotid stenosis: the tromso study. Circulation 103:2171–2175
31. Larsson M, Kremer F, Claus P, Kuznetsova T, Brodin LA, D'Hooge J (2011) Ultrasound-based radial and longitudinal strain estimation of the carotid artery: a feasibility study. IEEE Trans Ultrason Ferroelectr Freq Control 58:2244–2251
32. Le Floc'h S, Ohayon J, Tracqui P et al (2009) Vulnerable atherosclerotic plaque elasticity reconstruction based on a segmentation-driven optimization procedure using strain measurements: theoretical framework. IEEE Trans Med Imaging 28:1126–1137